Lattice stability and the effect of Co and Re on the ideal strength of Ni: First-principles study of uniaxial tensile deformation*

Minru Wen(文敏儒) and Chong-Yu Wang(王崇愚)†

Department of Physics, Tsinghua University, Beijing 100084, *China*

(Received 11 June 2017; published online 31 July 2017)

Using first-principles density functional calculations, lattice stability of γ-Ni under [001], [110], and [111] uniaxial tensions and the effect of alloying elements Co and Re on the uniaxial tensile behavior of γ-Ni were studied in this paper. With elastic constants and phonon spectra calculations, we examined the mechanical stability and phonon stability of Ni during the uniaxial tensions along the three characteristic directions. The results show that the mechanical stability and phonon stability of a lattice occurs before the maximum stress–strain point under the [001] and [111] tension, respectively. The effects of Co and Re on the ideal tensile strength of γ-Ni show a significant directivity: Co and Re have little effect on the stresses in [001] and [111] directions, but increases the ideal strength of the system in the weakest uniaxial tensile direction. Moreover, the strengthening effect of Re is significantly better than that of Co. By further analyzing electronic structure, it is found that the effect of alloying elements on the uniaxial tensile behavior of γ-Ni comes from their interactions with host atoms.

Keywords: lattice stability, first-principles, alloying elements, uniaxial tension

PACS: 31.15.es, 63.20.dk, 61.66.Dk, 62.20.F– **DOI:** 10.1088/1674-1056/26/9/093106

1. Introduction

The ideal strength of solid materials is the minimum stress required to make a defect-free crystal instable.[1,2] The ideal strength, which is related to the fracture of chemical bond and the initiation of cracks and dislocations, is an intrinsic mechanical parameter of the crystal material. Besides discussing the gap between the ideal strength and real strength of a material, the studying of ideal strength is also important for the investigation of fractures in applications.[2] For example, in some special materials, the width of the dislocation core is related to the size of its ideal shear strength, and the local stress of cleavage crack nucleation must be greater than its ideal uniaxial tensile strength.[3–5]

The ideal strength sets an upper bound for the strength of a real material. The simplest approach to determine the ideal strength is calculating the stress–strain curve of a system in the deformation process, and takes the first maximum or minimum point of the stress–strain curves as the ideal strength of materials.[6–14] Herein, the corresponding stress at this point is defined as the ideal peak stress ($\sigma_{\rm IP}$). However, instability in other forms may occur before the lattice reaches the ideal peak stress , such as mechanical instability (also known as elastic instability) and phonon instability (also known as dynamic instability). Born and Fürth[15,16] first proposed that a series of stability conditions should be examined during the deformation processes. These stability conditions are called the mechanical stability conditions (or elastic stability conditions), which are obtained by the positive definiteness of the elastic stiffness coefficient matrix. Mechanical stability is examined for many crystal structures.[17–26] Milstein and Farber[25] found that Fe and Ni have an elastic instability mode of $C_{22} = C_{23}$ before reaching their stress–strain maximum when they studied the phase transition of Fe and Ni under [100] tensile loading. Breidi *et al.*[24] also verified the mechanical stability during compression when they studied the $\langle 001 \rangle$ uniaxial compression of FCC-Ni , and found that the mechanical instability occurs after the ideal peak stress.

Mechanical stability considers the lattice stability of adjacent atoms in crystal under the action of central force, which is related to the macroscopic deformation of crystal. However, microscopic deformation in a solid material, such as soft phonon, may also reduce the energy of crystal.[2,28–30] This microscopic deformation leads to spatially periodic lattice distortion, which reduces the energy of crystal and results in lattice instability. In the first-principles calculations, soft phonon corresponds to the virtual frequency phonon, and such lattice instability is called phonon instability. Clatterbuck *et al.*[6] found that the phonon instability of a lattice occurs earlier than the maximum point of its stress–strain curve for Al during the $\langle 100 \rangle$, $\langle 110 \rangle$, and $\langle 111 \rangle$ tensile and $\{111\}$ $\langle 112 \rangle$ shear processes. It can be seen that calculating other instability (such as mechanical instability and phonon instability) in crystal deformation is very important for the study of ideal strength. However, no theoretical study has focused on the lattice stability of

*Project supported by Beijing Municipality Science and Technology Commission, China (Grant No. D161100002416001) and the National Key R&D Program of China (Grant No. 2017YFB0701502).

†Corresponding author. E-mail: cywang@mail.tsinghua.edu.cn

© 2017 Chinese Physical Society and IOP Publishing Ltd

Ni under the ⟨110⟩ and ⟨111⟩ uniaxial tensions.

As important structural materials, nickel-based single-crystal superalloys have been widely used as turbine blades for advanced aeroplanes and gas turbines.[31,32] A variety of alloying elements (such as Ta, W, Ti, Co, Cr, Re, Mo, and Ru) are added to modern commercial nickel-based superalloys to improve mechanical properties of alloys. The investigation of mechanical properties of γ-Ni, which is the matrix phase in nickel-based single-crystal superalloys, is extremely important for the applications of alloys. Previous studies of the effects of alloying elements on the mechanical properties mainly focus on the elastic constants and modulus.[33–37] However, scant attention has been paid to the ideal strength. In fact, alloying elements can have a significant influence on the strength of alloys.[38–40]

Using the first-principles calculations and combining with mechanical stability and phonon stability examinations, this paper studied uniaxial tensile behaviors of γ-Ni along the [001], [110], and [111] directions and the effects of alloying element Re and Co on the ideal tensile strength of γ-Ni. Furthermore, the electronic mechanism underlying the strengthening effect of Re and Co is determined by analyzing the charge density difference.

2. Computational methodology

For uniaxial tensile deformation, the stress σ is obtained from the derivation of energy to strain

$$\sigma = \frac{1}{V(\varepsilon)}\frac{\partial E(\varepsilon)}{\partial \varepsilon}, \tag{1}$$

where $E(\varepsilon)$ and $V(\varepsilon)$ are the total energy and the volume of a crystal when strain is ε. To simulate the stress–strain curve, we apply an increasing uniaxial tensile strain to crystals. The lattice basis vectors perpendicular to the loading direction were sufficiently relaxed. To ensure the continuity of stress–strain curves, the initial atomic positions of each step in the deformation process are taken from the relaxed configurations of the previous step.

For a crystal under zero loading, the mechanical stability criteria can be expressed in terms of elastic constants.[41]

$$\det|C_{ijkl}| > 0, \tag{2}$$

where $C_{ijkl} = \frac{1}{V}\frac{\partial^2 F}{\partial \varepsilon_{ij}\partial \varepsilon_{kl}}$ is the second-order elastic constant, F is the free energy of a crystal, ε_{ij} and ε_{kl} (where $i,j,k,l = \{1,2,3\}$) are the infinitesimal strains. Under an external loading τ_{ij}, the elastic stability criteria need to be modified since the elastic constants are dependent on the applied stress[42]

$$\det|B_{ijkl}| > 0, \tag{3}$$

where $B_{ijkl} = C_{ijkl} + \frac{1}{2}(\delta_{ik}\tau_{jl} + \delta_{il}\tau_{jk} + \delta_{jk}\tau_{il} + \delta_{jl}\tau_{ik} - 2\delta_{kl}\tau_{ij})$ is the elastic stiffness constant. In general, the elastic stiffness constant is asymmetric (i.e., $B_{ijkl} \neq B_{klij}$) and does not have full Voigt symmetry. By introducing a new tensor λ [23]

$$\begin{aligned}\lambda_{ijkl} &= \frac{1}{2}(B_{ijkl} + B_{klij}) \\ &= C_{ijkl} + \frac{1}{2}(\delta_{ik}\tau_{jl} + \delta_{il}\tau_{jk} + \delta_{jk}\tau_{il} \\ &\quad + \delta_{jl}\tau_{ik} - \delta_{kl}\tau_{ij} - \delta_{ij}\tau_{kl}),\end{aligned} \tag{4}$$

we get a symmetric tensor λ. The tensor λ has full Voigt symmetry and its positive definiteness is the same as that of the elastic stiffness tensor. Consequently, by using Voigt notation ($11 \to 1$, $22 \to 2$, $33 \to 3$, $23 \to 4$, $13 \to 5$, $12 \to 6$),[43] the conditions of elastic stability can also be expressed in the elements of λ

$$\det|\lambda_{\alpha\beta}| > 0, \tag{5}$$

where $\alpha,\beta = \{1,2,3,4,5,6\}$.

Under a [100] uniaxial loading,

$$\tau = \begin{bmatrix} \sigma & 0 & 0 \\ 0 & 0 & 0 \\ 0 & 0 & 0 \end{bmatrix},$$

initial FCC-Ni becomes tetragonal ($422, 4mm, \bar{4}2m, 4/mmm$) and the tensor λ takes the following form:

$$\{\lambda_{\alpha\beta}\} = \begin{pmatrix} \lambda_{11} & \lambda_{12} & \lambda_{12} & 0 & 0 & 0 \\ \lambda_{12} & \lambda_{22} & \lambda_{23} & 0 & 0 & 0 \\ \lambda_{12} & \lambda_{23} & \lambda_{22} & 0 & 0 & 0 \\ 0 & 0 & 0 & \lambda_{44} & 0 & 0 \\ 0 & 0 & 0 & 0 & \lambda_{55} & 0 \\ 0 & 0 & 0 & 0 & 0 & \lambda_{55} \end{pmatrix}. \tag{6}$$

According to Eq. (4), the relation between $\lambda_{\alpha\beta}$ and $C_{\alpha\beta}$ is

$$\begin{cases} \lambda_{11} = C_{11} + \sigma, \\ \lambda_{12} = C_{12} - \sigma/2, \\ \lambda_{55} = C_{55} + \sigma/2, \\ \lambda_{\alpha\beta} = C_{\alpha\beta}, \quad \text{all others.} \end{cases} \tag{7}$$

The determinant of λ is

$$\det|\lambda| = (\lambda_{22} - \lambda_{23})[\lambda_{11}(\lambda_{22} + \lambda_{23}) - 2\lambda_{12}^2]\lambda_{44}\lambda_{55}^2. \tag{8}$$

Consequently, the elastic stability criteria of tetragonal lattice under [100] uniaxial stress are

$$\lambda_{44} > 0 \Rightarrow C_{44} > 0, \tag{9a}$$

$$\lambda_{55} > 0 \Rightarrow C_{55} + \frac{\sigma}{2} > 0, \tag{9b}$$

$$\lambda_{22} - \lambda_{23} > 0 \Rightarrow C_{22} - C_{23} > 0, \tag{9c}$$

$$\lambda_{11}(\lambda_{22} + \lambda_{23}) > 2\lambda_{12}^2 \Rightarrow (C_{11} + \sigma)(C_{22} + C_{23}) > 2\left(C_{12} - \frac{\sigma}{2}\right)^2. \tag{9d}$$

Under a [110] uniaxial tension

$$\tau = \begin{bmatrix} \frac{\sqrt{2}}{2}\sigma & 0 & 0 \\ 0 & \frac{\sqrt{2}}{2}\sigma & 0 \\ 0 & 0 & 0 \end{bmatrix},$$

and [111] tension

$$\tau = \begin{bmatrix} \frac{\sqrt{3}}{3}\sigma & 0 & 0 \\ 0 & \frac{\sqrt{3}}{3}\sigma & 0 \\ 0 & 0 & \frac{\sqrt{3}}{3}\sigma \end{bmatrix},$$

an initial FCC-Ni becomes orthorhombic and trigonal (32, $\bar{3}m$, $3m$). The corresponding tensor λ takes the following form:

$$\{\lambda_{\alpha\beta}\} = \begin{pmatrix} \lambda_{11} & \lambda_{12} & \lambda_{13} & 0 & 0 & 0 \\ \lambda_{12} & \lambda_{22} & \lambda_{23} & 0 & 0 & 0 \\ \lambda_{13} & \lambda_{23} & \lambda_{33} & 0 & 0 & 0 \\ 0 & 0 & 0 & \lambda_{44} & 0 & 0 \\ 0 & 0 & 0 & 0 & \lambda_{55} & 0 \\ 0 & 0 & 0 & 0 & 0 & \lambda_{66} \end{pmatrix}, \quad (10)$$

$$\{\lambda_{\alpha\beta}\} = \begin{pmatrix} \lambda_{11} & \lambda_{12} & \lambda_{13} & \lambda_{14} & 0 & 0 \\ \lambda_{12} & \lambda_{11} & \lambda_{13} & -\lambda_{14} & 0 & 0 \\ \lambda_{13} & \lambda_{13} & \lambda_{33} & 0 & 0 & 0 \\ \lambda_{14} & -\lambda_{14} & 0 & \lambda_{44} & 0 & 0 \\ 0 & 0 & 0 & 0 & \lambda_{44} & \lambda_{14} \\ 0 & 0 & 0 & 0 & \lambda_{14} & (\lambda_{11}-\lambda_{12})/2 \end{pmatrix} \quad (11)$$

for orthorhombic and trigonal (32, $\bar{3}m$, $3m$) lattice, respectively.

Similar to the [100] tension, we obtain the relation between $\lambda_{\alpha\beta}$ and $C_{\alpha\beta}$ of orthorhombic lattice under [110] tension as

$$\begin{cases} \lambda_{11} = C_{11} + \frac{\sqrt{2}}{2}\sigma, \lambda_{12} = C_{12} - \frac{\sqrt{2}}{2}\sigma, \lambda_{13} = C_{13} - \frac{\sqrt{2}}{4}\sigma, \\ \lambda_{22} = C_{22} + \frac{\sqrt{2}}{2}\sigma, \lambda_{23} = C_{23} - \frac{\sqrt{2}}{4}\sigma, \lambda_{33} = C_{33}, \\ \lambda_{44} = C_{44} + \frac{\sqrt{2}}{4}\sigma, \lambda_{55} = C_{55} + \frac{\sqrt{2}}{4}\sigma, \lambda_{66} = C_{66} + \frac{\sqrt{2}}{2}\sigma. \end{cases} \quad (12)$$

Thus, the mechanical stability criteria of an orthorhombic lattice are

$$\lambda_{11} > 0 \Rightarrow C_{11} + \frac{\sqrt{2}}{2}\sigma > 0, \quad (13a)$$

$$\lambda_{44} > 0 \Rightarrow C_{44} + \frac{\sqrt{2}}{4}\sigma > 0, \quad (13b)$$

$$\lambda_{55} > 0 \Rightarrow C_{55} + \frac{\sqrt{2}}{4}\sigma > 0, \quad (13c)$$

$$\lambda_{66} > 0 \Rightarrow C_{66} + \frac{\sqrt{2}}{2}\sigma > 0, \quad (13d)$$

$$\lambda_{11}\lambda_{22} > \lambda_{12}^2 \Rightarrow \left(C_{11} + \frac{\sqrt{2}}{2}\sigma\right)\left(C_{22} + \frac{\sqrt{2}}{2}\sigma\right) > \left(C_{12} - \frac{\sqrt{2}}{2}\sigma\right)^2, \quad (13e)$$

$$\lambda_{11}\lambda_{22}\lambda_{33} + 2\lambda_{12}\lambda_{13}\lambda_{23} - \lambda_{11}\lambda_{23}^2 - \lambda_{22}\lambda_{13}^2 - \lambda_{33}\lambda_{12}^2 > 0 \Rightarrow$$
$$\left(C_{11} + \frac{\sqrt{2}}{2}\sigma\right)\left(C_{22} + \frac{\sqrt{2}}{2}\sigma\right)C_{33}$$
$$+2\left(C_{12} - \frac{\sqrt{2}}{2}\sigma\right)\left(C_{13} - \frac{\sqrt{2}}{4}\sigma\right)\left(C_{23} - \frac{\sqrt{2}}{4}\sigma\right)$$
$$-\left(C_{11} + \frac{\sqrt{2}}{2}\sigma\right)\left(C_{23} - \frac{\sqrt{2}}{4}\sigma\right)^2$$
$$-\left(C_{22} + \frac{\sqrt{2}}{2}\sigma\right)\left(C_{13} - \frac{\sqrt{2}}{4}\sigma\right)^2$$
$$-C_{33}\left(C_{12} - \frac{\sqrt{2}}{2}\sigma\right)^2 > 0. \quad (13f)$$

Finally, the relations between the $\lambda_{\alpha\beta}$ and $C_{\alpha\beta}$ of the trigonal lattice under [111] tension are

$$\begin{cases} \lambda_{11} = C_{11} + \frac{\sqrt{3}}{3}\sigma, \lambda_{12} = C_{12} - \frac{\sqrt{3}}{3}\sigma, \lambda_{13} = C_{13} - \frac{\sqrt{3}}{3}\sigma, \\ \lambda_{33} = C_{33} + \frac{\sqrt{3}}{3}\sigma, \lambda_{14} = C_{14}, \lambda_{44} = C_{44} + \frac{\sqrt{3}}{3}\sigma. \end{cases} \quad (14)$$

The corresponding mechanical stability criteria of a trigonal lattice are given by

$$\lambda_{11} > |\lambda_{12}| \Rightarrow C_{11} + \frac{\sqrt{3}}{3}\sigma > |C_{11} - \frac{\sqrt{3}}{3}\sigma|, \quad (15a)$$

$$\lambda_{33} > 0 \Rightarrow C_{33} + \frac{\sqrt{3}}{3}\sigma > 0, \quad (15b)$$

$$\lambda_{44} > 0 \Rightarrow C_{44} + \frac{\sqrt{3}}{3}\sigma > 0, \quad (15c)$$

$$(\lambda_{11} + \lambda_{12})\lambda_{33} > 2\lambda_{13}^2 \Rightarrow (C_{11} + C_{12})\left(C_{33} + \frac{\sqrt{3}}{3}\sigma'\right) > 2\left(C_{13} - \frac{\sqrt{3}}{3}\sigma\right)^2, \quad (15d)$$

$$\lambda_{11} - \lambda_{12})\lambda_{44} > 2\lambda_{14}^2 \Rightarrow \left(C_{11} + C_{12} + \frac{2\sqrt{3}}{3}\sigma\right)\left(C_{44} + \frac{\sqrt{3}}{3}\sigma\right) > 2C_{14}^2. \quad (15e)$$

To test the mechanical stability of a lattice during the tensile processes, we calculate the elastic constants C_{ij} of the lattice at every tensile strain and examine the mechanical stability conditions for the corresponding crystal according to Eqs. (9), (13), and (15). To calculate elastic constants of tetragonal, orthorhombic, and trigonal crystals, we apply specific deformation tensors listed in Ref. [44] to each crystal and calculate the energy–strain relationship, where the deformation parameter δ increases from -0.03 to 0.03 in steps of 0.005. Then the elastic constant of each crystal is obtained by fitting the energy–strain curve by polynomial.

In the present study, we adopt a $2 \times 2 \times 2$ supercell model to investigate the effect of alloying elements Re and Co on the uniaxial tensile behavior of γ-Ni. The alloying elements are located at the center of the supercell. Based on the density functional theory (DFT),[45,46] our calculations are carried out using the VASP package.[47] The generalized gradient approximation of PBE potential[48] is used to describe the exchange-correlation function. The projector augmented wave (PAW) method[49] is used to describe the ion–electron interaction. The plane wave cutoff is set to 350 eV. Following the Monkhorst–Pack scheme,[50] we adopt an $11 \times 11 \times$

11 k-point mesh. The convergence condition of electron self-consistent energy is 10^{-5} eV. The ionic relaxation is stopped until the forces on all of the atoms are less than 0.01 eV/Å.

The phonon spectrum is calculated with the density functional perturbation theory,[51] which was achieved via VASP-PHONOPY using a $2 \times 2 \times 2$ supercell.[47,52,53] As the phonon spectrum calculation requires high precision, 500 eV is taken as the plane wave cutoff and the k-point mesh is $11 \times 11 \times 11$ for phonon calculations. The convergence conditions of electron self-consistent and ionic relaxation are 10^{-8} eV and 10^{-7} eV, respectively.

3. Results and discussion

3.1. Lattice stability of Ni under uniaxial tensile deformation

The energy–strain relationships of γ-Ni under [001], [110], and [111] tensile loadings are shown in Fig. 1(a), and the corresponding stress–strain curves (Fig. 1(b)) are obtained by Eq. (1). As shown in Fig. 1, the energy and stress of γ-Ni under [001] uniaxial tension increase with the increase in strain. At the strain $\varepsilon = 0.32$, the stress reaches the maximum value of 26.76 GPa. This point is the ideal peak stress $\sigma_{\rm IP}$ in the [001] direction. Similar to the [001] direction, the stress reaches the ideal peak stress of 26.61 GPa at the strain of 0.22 under [111] tension. For the [110] tensile process, the stress of Ni gets its peak point at small strain ($\varepsilon = 0.08$), and its ideal peak stress is only 6.03 GPa. Obviously, compared to the large $\sigma_{\rm IP}$ in [001] and [111] directions, [110] is the weakest uniaxial tensile direction for γ-Ni. Table 1 summarizes our calculated ideal peak stresses of γ-Ni in [001], [110], and [111] directions along with calculation results of Milstein *et al.*[25] As shown in the table, our calculated results are in good agreement with that of Milstein *et al.*[25]

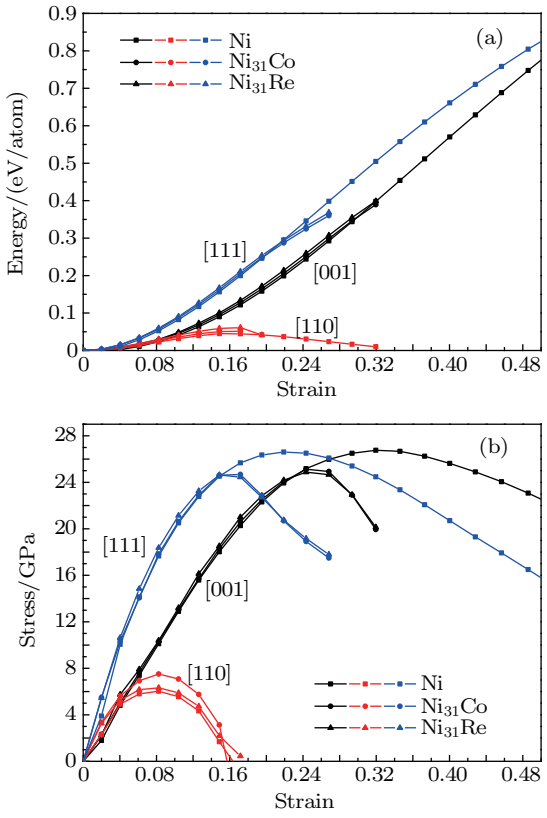


Fig. 1. (color online) (a) Energy–strain curve and (b) stress–strain curve of $Ni_{31}X$ (X = Ni, Co, and Re). The black, red, and blue data represent the [001], [110], and [111] tension, respectively.

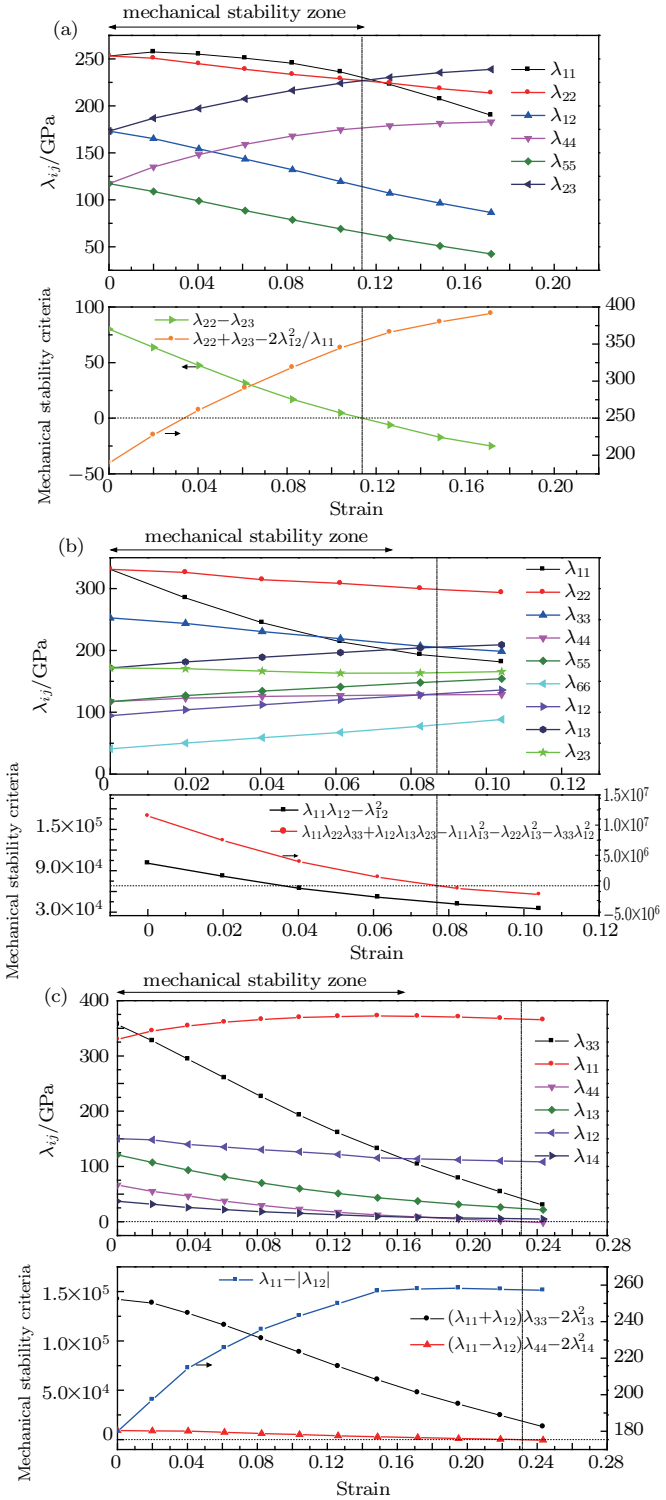


Fig. 2. (color online) (a)–(c) Element of tensor λ (upper half) and the corresponding mechanical stability conditions (lower half) of γ-Ni under [001], [110], and [111] tension, respectively. The vertical dashed line marks the maximum mechanical stability point of the lattice.

Furthermore, we calculate elastic constants of the lattice during the tensile tests to examine the mechanical stability conditions of crystal (Eqs. (9), (13), and (15)). Figures 2(a)–2(c) show λ_{ij} and the corresponding mechanical stability criteria of crystal along the [001], [110], and [111] loading, respectively. As shown in Fig. 2(a), when the strain is not applied to the lattice, the crystal only has three independent λ_{ij}: $\lambda_{11} = \lambda_{22}$, $\lambda_{12} = \lambda_{23}$, and $\lambda_{44} = \lambda_{55}$. As loading strain ε increases in the [001] direction, elastic modulus λ_{11}, λ_{22}, λ_{12}, and λ_{55} decrease, and λ_{44} and λ_{23} increase. When tensile strain $\varepsilon = 0.11$, λ_{22} is equal to λ_{23}. After this strain ($\varepsilon > 0.11$), the elastic modulus λ_{22} is less than λ_{23} and the mechanical stability condition Eq. (9c) of the tetragonal system is invalid. Herein, the corresponding point and stress at which the mechanical stability conditions are first violated are defined as the maximum mechanical stability point and maximum mechanical stability stress (σ_{MMS}). As shown in Fig. 1(b), the stress at the strain $\varepsilon = 0.11$ is 14.11 GPa under [001] tension, so the maximum mechanical stability stress of [001] uniaxial tension is $\sigma_{\mathrm{MMS}} = 14.11$ GPa. Similarly, as shown in Figs. 2(b) and 2(c), the maximum mechanical stability points are at $\varepsilon = 0.07$ and $\varepsilon = 0.23$ during tension in the [110] and [111] directions, respectively. The instability modes are $\lambda_{11}\lambda_{22}\lambda_{33} + 2\lambda_{12}\lambda_{13}\lambda_{23} - \lambda_{11}\lambda_{23}^2 - \lambda_{22}\lambda_{13}^2 - \lambda_{33}\lambda_{12}^2 = 0$ and $\lambda_{44} = 0$ for [110] and [111] loading, respectively. Correspondingly, the maximum mechanical stability stresses in the [110] and [111] directions are 6.03 GPa and 25.56 GPa, respectively, according to Fig. 1(b).

Table 1. Calculated ideal peak stress σ_{IP}, maximum mechanical stability stress σ_{MMS}, and maximum phonon stability stress σ_{MPS} of γ-Ni under [001], [110], and [111] tensions. Numbers in round brackets represent the strain corresponding to each stress.

Directions	$\sigma_{\mathrm{IP}}(\varepsilon)$	$\sigma_{\mathrm{MMS}}(\varepsilon)$	$\sigma_{\mathrm{MPS}}(\varepsilon)$
[001]	26.76 (0.32)	14.11 (0.11)	21.90(0.19)
	25.75 (0.26)[25]	17.03 (0.11)[25]	–
[110]	6.03 (0.08)	6.03 (0.08)	4.68(0.12)
[111]	26.61 (0.22)	26.56 (0.23)	25.47(0.17)

Furthermore, we calculate the phonon spectra of γ-Ni during the tensile loading in [001], [110], and [111] directions to examine the phonon stability. Figures 3(a)–3(c) show phonon frequencies of γ-Ni as a function of strain for [001], [110], and [111] tension, respectively. Note that we have included only the first band and the high symmetry directions in the Brillouin zone along which phonon instabilities are found to occur. As shown in Fig. 3(a), a softening occurs between $\Gamma \to X$ ($q = [0.5, 0.5, 1]$) as the tensile strain ε increases in the [001] direction. When $\varepsilon = 0.19$, imaginary frequency first occurs in Fig. 3(a), which is exactly the phonon instability point of the system. Herein, the corresponding stress and strain at which the phonon frequency is firstly imaginary is defined as the maximum phonon stability stress (σ_{MPS}) and maximum mechanical stability strain ($\varepsilon_{\mathrm{MPS}}$), respectively. As shown in Figs. 1 and 2, the phonon instability point in the [001] direction occurs earlier than that of the peak stress point, but later than the occurrence of the mechanical instability point. Similarly, it can be seen from Figs. 3(b) and 3(c) that phonon instability of Ni occurs at $\varepsilon = 0.12$ and $\varepsilon = 0.17$ during tension along the [110] and [111] directions, respectively.

Table 1 summarizes σ_{IP}, σ_{MMS}, and σ_{MPS} along with their corresponding strain for γ-Ni under the [001], [110], and [111] tensile deformations. It can be seen that $\varepsilon_{\mathrm{MMS}} < \varepsilon_{\mathrm{MPS}} < \varepsilon_{\mathrm{IS}}$ for [001] tension and $\varepsilon_{\mathrm{MPS}} < \varepsilon_{\mathrm{IS}} < \varepsilon_{\mathrm{MMS}}$ for [111] tension. Therefore, the ideal strength σ_{IS} of Ni under [001] and [111] tensions is determined by the σ_{MMS} and σ_{MPS}, respectively. Unlike the [001] and [111] directions, the lattice instability point of Ni under [110] loading is equal to its ideal peak point. After considering mechanical stability and phonon stability of lattice during the deformations, the ideal tensile strengths of γ-Ni in [001], [110], and [111] directions are 14.11 GPa, 6.03 GPa, and 25.47 GPa, respectively.

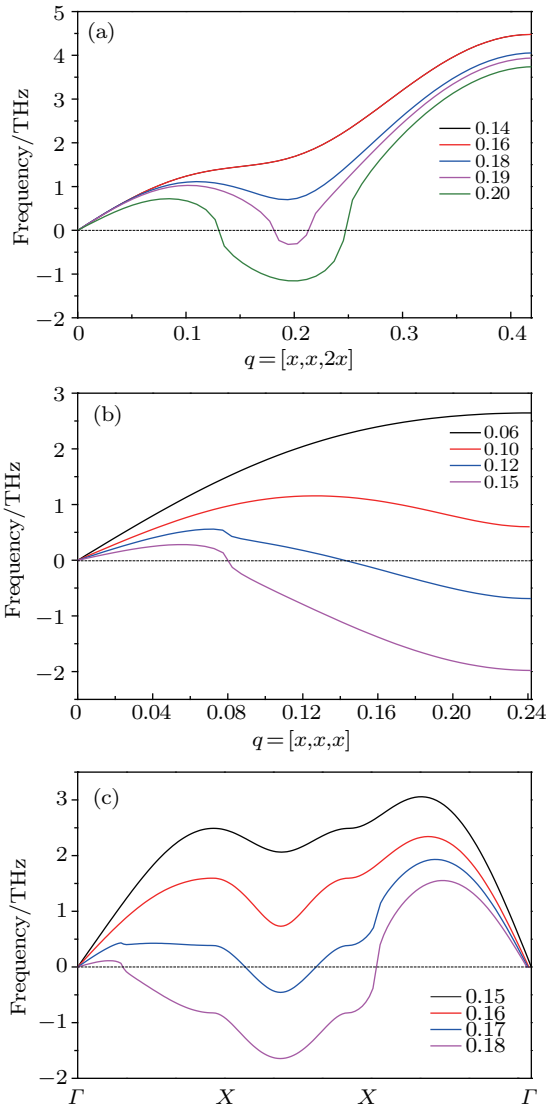


Fig. 3. (color online) (a)–(c) First band of phonon of γ-Ni as a function of strain for [001], [110], and [111] tension, respectively.

3.2. Effects of Re and Co on the ideal tensile strength

The response of energy and stress to strain for $Ni_{31}Co$ and $Ni_{31}Re$ are also shown in Fig. 1. As shown in the figure, effects of alloying elements Co and Re on the stress show obvious directionality. Compared to the stress of pure Ni, stresses of $Ni_{31}Co$ and $Ni_{31}Re$ show only a very small increase before the yield point for the [001] and [111] directions. Note that by doping with Co and Re, the systems reach their ideal peak stress at a smaller strain as compared with pure γ-Ni. Therefore, doping with Co and Re decreases the ideal peak stress of the system. Unlike the [001] and [111] directions, doping with Co and Re can significantly increase the ideal peak stress in the [110] direction. The value of σ_{IP} in the [110] direction increases from 6.03 GPa to 6.32 GPa for $Ni_{31}Co$ and to 7.50 GPa for $Ni_{31}Re$. It can be seen that refractory elements Co and Re can significantly improve the ideal strength of γ-Ni in the weakest tensile direction, and the strengthening effect of Re is significantly stronger than that of Co.

To understand the different improvements due to Co and Re on the weakest tensile direction and the anisotropy effects of alloying elements on the ideal strength, we further calculate and analyze the charge density difference ($\Delta\rho$) of $Ni_{31}X$. Charge density difference reflects the charge transfer before and after atomic bonding, which shows the interaction between atoms. Figures 4(a)–4(c) show the charge density difference of $Ni_{31}X$ (X = Ni, Co, and Re) without strain loaded, where yellow and cyan isosurface represents charge accumulation and depletion, respectively. As shown in Fig. 4, the $\Delta\rho$ of $Ni_{31}Co$ exhibits nearly the same feature as the $\Delta\rho$ of un-doped Ni. However, there is a strong redistribution of charge density around Re atoms in $Ni_{31}Re$. Moreover, the charge redistribution in $Ni_{31}Re$ shows obvious directionality: $\Delta\rho$ mainly accumulates between Re and the host atoms (i.e., in the [110] direction), while there is very little charge redistribution in the [001] and [111] directions. In addition, the bonding between Re and Ni atoms significantly exhibits covalent-like bond features. This feature of charge redistribution suggests that the addition of refractory element Re can enhance bonding in the [110] direction and has little effect on the bonding of [001] and [111] directions. This is consistent with the results of our calculated stress–strain curves (Fig. 1(b)). The strengthening effect of Re on the ideal strength along the [110] direction is significantly greater than that of Co, but enhancement in [001] and [111] directions is negligible.

Figures 4(d)–4(f) show $\Delta\rho$ of $Ni_{31}Re$ under tension along the [001], [110], and [111] directions at strain $\varepsilon = 0.06$, respectively. As shown in Figs. 4(d)–4(f), the redistribution of charge density of $Ni_{31}Re$ decreases in the loading direction for the three characteristic directional deformations. However, although under the same tensile strain, the decrease of $\Delta\rho$ in the loading direction varies to certain extents for the three characteristic directions. The decrease of $\Delta\rho$ caused by the [110] tension is the largest, followed by that due to the [111] tension, and variation of $\Delta\rho$ caused by [001] loading is the weakest. It can be implied that the deformation resistance of $Ni_{31}Re$ in [001] and [111] directions is obviously better than that in the [110] direction. This is consistent with the previous results of stress–strain curves (Fig. 1(b)): the yield point of [110] tension occurs much earlier than those of the [001] and [111] tensions.

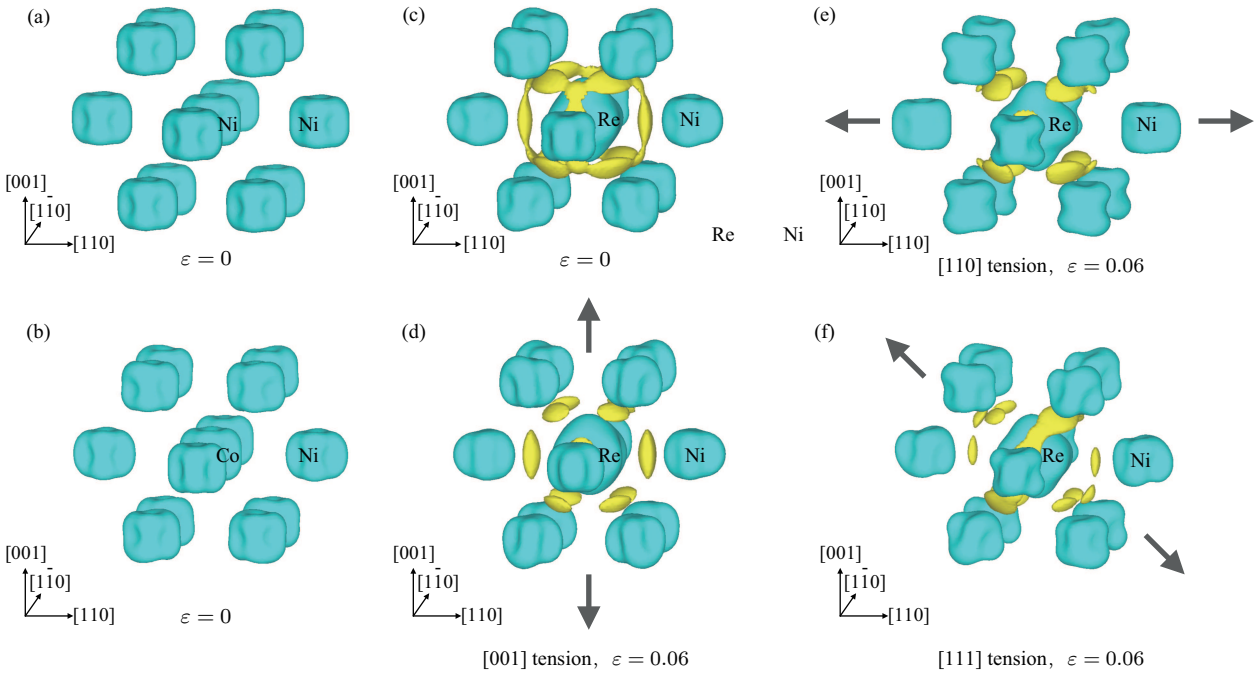


Fig. 4. (color online) Charge density differences of $Ni_{31}X$ (isosurface ± 0.0695 e/Å^3). (a) X = Ni, $\varepsilon = 0.00$; (b) X = Co, $\varepsilon = 0.00$; (c) X = Re, $\varepsilon = 0.00$; (d) X = Re, $\varepsilon = 0.06$, [001] tension; (e) X = Re, $\varepsilon = 0.06$, [110] tension; (f) X = Re, $\varepsilon = 0.06$, [111] tension. Yellow (cyan) isosurface represents charge accumulation (depletion). Each structure is a central X atom surrounded by 12 Ni atoms.

4. Conclusions

Using density functional theory, we studied the lattice stability and the effect of alloying elements on the tensile strength of γ-Ni under three uniaxial characteristic directions. With mechanical stability and phonon stability examinations, it is found that mechanical instability and phonon instability of γ-Ni under uniaxial tension occurs before the ideal peak stress for the [001] and [111] directions, respectively. The ideal tensile strengths of γ-Ni in [001], [110] and [111] directions are determined to be 14.11 GPa, 6.03 GPa, and 25.47 GPa, respectively. Doping with Co and Re can increase the ideal peak stress of γ-Ni in the [110] direction by 4.8% and 24.4%, respectively. However, Re and Co have a negligible effect on the ideal strength in [001] and [111] directions. Further analysis of charge density difference of these alloying systems showed that the effects of alloying elements on the uniaxial tensile behavior arise from their interaction with host atoms. There is a strong charge redistribution around the Re atom along the $\langle 110 \rangle$ direction in $Ni_{31}Re$, while charge redistribution of $Ni_{31}Co$ is nearly the same as that of un-doped Ni.

Acknowledgment

The simulations were carried out on the "Explorer 100" cluster system of the Tsinghua National Laboratory for Information Science and Technology, Beijing, China.

References

[1] Kelly A and Macmillan N H 1986 *Strong Solids*, 3rd edn (Oxford: Clarendon Press)
[2] Pokluda J, Černý M, Šob M and Umeno Y 2015 *Prog. Mater. Sci.* **73** 127
[3] Krenn C R, Roundy D, Morris J W and Cohen M L 2001 *Mater. Sci. Eng.: A* **319** 111
[4] Chrzan D C, Sherburne M P, Hanlumyuang Y, Li T and Morris Jr J W 2010 *Phys. Rev. B* **82** 184202
[5] Sawyer C A, Morris Jr J W and Chrzan D C 2013 *Phys. Rev. B* **87** 134106
[6] Clatterbuck D M, Krenn C R, Cohen M L and Morris Jr J W 2003 *Phys. Rev. Lett.* **91** 135501
[7] Ogata S, Li J and Yip S 2002 *Science* **298** 807
[8] Clatterbuck D M, Chrzan D C and Morris J W 2003 *Acta Mater.* **51** 2271
[9] Ogata S, Li J, Hirosaki N, Shibutani Y and Yip S 2004 *Phys. Rev. B* **70** 104104
[10] Liu Y L, Zhang Y, Zhou H B, Lu G H and Kohyama M 2008 *J. Phys.: Condens. Matter* **20** 335216
[11] Wu X and Wang C 2016 *RSC Adv.* **6** 20551
[12] Shang S L, Wang W Y, Wang Y, Du Y, Zhang J X, Patel A D and Liu Z K 2012 *J. Phys.: Condens. Matter* **24** 155402
[13] Liu Y L, Zhang Y, Hong R J and Lu G H 2009 *Chin. Phys. B* **18** 1923
[14] Zhang C L, Han P D, Wang X H, Zhang Z X, Wang L P and Xu H X 2013 *Chin. Phys. B* **22** 126802
[15] Born M and Fürth R 1940 *MPCPS*, pp. 454–465
[16] Born M 1940 *MPCPS*, pp. 160–172
[17] Pokluda J, Černý M, Šandera P and Šob M 2004 *J. Comput. Aided Mater. Des.* **11** 1-28
[18] Hill R and Milstein F 1977 *Phys. Rev. B* **15** 3087
[19] Milstein F 1971 *Phys. Rev. B* **3** 1130
[20] Wang J, Li J, Yip S, Phillpot S and Wolf D 1995 *Phys. Rev. B* **52** 12627
[21] Wang J, Yip S, Phillpot S R and Wolf D 1993 *Phys. Rev. Lett.* **71** 4182
[22] Zhou Z and Joós B 1996 *Phys. Rev. B* **54** 3841
[23] Morris J W and Krenn C R 2000 *Philos. Mag. A* **80** 2827
[24] Breidi A, Fries S G and Ruban A V 2016 *Phys. Rev. B* **93** 144106
[25] Milstein F and Farber B 1980 *Phys. Rev. Lett.* **44** 277
[26] Řehák P, Černý M and Šob M 2015 *Modell. Simul. Mater. Sci. Eng.* **23** 055010
[27] Mouhat F and Coudert F X 2014 *Phys. Rev. B* **90** 224104
[28] Zhao G L and Harmon B N 1992 *Phys. Rev. B* **45** 2818
[29] Reháy P, Cerný M and Pokluda J 2012 *J. Phys.: Condens. Matter* **24** 215403
[30] Miao L, Liu H J, Hu Y, Zhou X, Hu C Z and Shi J 2010 *Chin. Phys. B* **19** 016301
[31] Reed R C 2006 *The Superalloys: Fundamentals and Applications* (New York: Cambridge university press)
[32] Reed R, Tao T and Warnken N 2009 *Acta Mater.* **57** 5898
[33] Kim D, Shang S L and Liu Z K 2009 *Comput. Mater. Sci.* **47** 254
[34] Wang Y, Wang J J, Zhang H, Manga V R, Shang S L, Chen L Q and Liu Z K 2010 *J. Phys.: Condens. Matter* **22** 225404
[35] Shang S L, Kim D E, Zacherl C L, Wang Y, Du Y and Liu Z K 2012 *J. Appl. Phys.* **112** 053515
[36] Wu X and Wang C 2015 *J. Phys.: Condens. Matter* **27** 295401
[37] Wang Y and Wang C 2009 *MRS Proceedings*, pp. 1224-FF1205-1231
[38] Yeh A C and Tin S 2005 *Scripta Mater.* **52** 519
[39] Tian C, Han G, Cui C and Sun X 2015 *Mater. Des.* **88** 123
[40] Fleischmann E, Miller M K, Affeldt E and Glatzel U 2015 *Acta Mater.* **87** 350
[41] Nye J F 1985 *Physical Properties of Crystals: their Representation by Tensors and Matrices* (New York: Oxford university press)
[42] Wallace D C 1998 *Thermodynamics of Crystals* (New York: Dover Publications)
[43] Voigt W 1928 *Lehrbuch der Kristallphysik* (Leipzig Berlin: Ann Arbor, Mich)
[44] Wen M and Wang C Y 2016 *RSC Adv.* **6** 77489
[45] Hohenberg P and Kohn W 1964 *Phys. Rev.* **136** B864
[46] Kohn W and Sham L J 1965 *Phys. Rev.* **140** A1133
[47] Kresse G and Furthmüller J 1996 *Phys. Rev. B* **54** 11169
[48] Perdew J P, Burke K and Ernzerhof M 1996 *Phys. Rev. Lett.* **77** 3865
[49] Kresse G and Joubert D 1999 *Phys. Rev. B* **59** 1758
[50] Monkhorst H J and Pack J D 1976 *Phys. Rev. B* **13** 5188
[51] Baroni S, De Gironcoli S, Dal Corso A and Giannozzi P 2001 *Rev. Mod. Phys.* **73** 515
[52] Togo A, Oba F and Tanaka I 2008 *Phys. Rev. B* **78** 134106
[53] Togo A and Tanaka I 2015 *Scripta Mater.* **108** 1